Electronic Supplementary Information

Periodic Law-Guided Design of Highly Stable O3-Type Layered Oxide Cathodes for Practical Sodium-Ion Batteries

Yuan-Bo Wu, [ab] Hai-Yan Hu, *[abc] Jia-Yang Li, [c] Hang-Hang Dong, [b] Yan-Fang Zhu, *[ab] Shuang-Qiang Chen, [ab] Na-Na Wang, [c] Jia-Zhao Wang, [b] Yao Xiao *[abd]

[a] College of Chemistry and Materials Engineering, Wenzhou University, Wenzhou, 325035, P. R. China.

E-mail: hyh927@uowmail.edu.au; yanfangzhu@wzu.edu.cn; xiaoyao@wzu.edu.cn

[b] Wenzhou Key Laboratory of Sodium-Ion Batteries, Wenzhou University Technology Innovation Institute for Carbon Neutralization, Wenzhou, 325035, P. R. China

[c] Institute for Superconducting and Electronic Materials Australian Institute for Innovative Materials University of Wollongong Innovation Campus, North Wollongong, NSW 2522, Australia

[d] Key Laboratory of Advanced Energy Materials Chemistry (Ministry of Education), Nankai University, Tianjin, 300071, P. R. China

Experimental Section

Materials synthesis. The O3-$NaNi_{0.4}Cu_{0.05}Mg_{0.05}Mn_{0.3}Ti_{0.2}O_2$ (NaNCMMT) samples were synthesized via high-temperature solid-state reaction using stoichiometric mixtures of Na_2CO_3 (99.5%, with 10 mol% excess; Alfa Aesar), NiO (99.0%; Alfa Aesar), CuO (99.7%; Sinopharm), MgO (99%; Alfa Aesar), Mn_2O_3 (98.0%; Alfa Aesar), and TiO_2 (anatase, 99.6%; Alfa Aesar). The powders were thoroughly ground and pressed into pellets under 16 MPa. These pellets were then calcined at 1000 ^oC in air for 15 hours, cooled to room temperature, and stored in an argon-filled glove box (H_2O and O_2 < 0.1 ppm). For comparison, O3-$NaNi_{0.5}Mn_{0.5}O_2$ (NaNM) samples were prepared using the same procedure. To evaluate moisture stability, the samples underwent a soaking process by immersing them in water for 10 minutes, followed by drying at 1000 ^oC for 12 hours.

Materials characterization. X-ray diffraction (XRD) patterns were collected using a PANalytical Aeris diffractometer with Cu Kα radiation (λ = 1.5406 Å) at 2^o min^{-1}. The crystal structure was analyzed via Rietveld refinement using Fullprof software. *In-situ* charge and discharge XRD was performed in a Swagelok cell with a Be foil X-ray window. X-ray photoelectron spectroscopy (XPS) was conducted on a Thermo Scientific Nexsa spectrometer. Infrared (IR) spectra were obtained using a FT-IR spectrophotometer with an MCT AIM-8800 detector. Differential electrochemical mass spectrometry (DEMS) was measured with an OmniStar GSD 320 instrument. Morphology and structure were characterized by scanning electron microscopy (SEM, JEOL 7500) and transmission electron microscopy (TEM, JEOL JEM-2011). The chemical composition was identified by inductively coupled plasma-mass spectrometry (ICP-MS). The X-ray absorption fine structure (XAFS) spectra at the Ni K-edge

of NaNCMMT was collected in transmission mode using a Table XAFS-500 (Specreation Instruments Co., Ltd.) operating at 25 kV and 20 mA. A Si (551) spherically bent crystal analyzer with a radius of curvature of 500 mm was used. Before the test, the samples were grinded and tableted into slices with a diameter of 12.7 mm. The sample was ground and pressed into pellets with a diameter of 12.7 mm for the measurement. Particle size distribution was determined using a laser particle size analyzer (BT-9300ST), and water sensitivity was assessed by dynamic contact angle testing (CA100D).

Electrochemical measurements. Electrochemical properties were assessed in CR2032 coin cells with Na disks as the anode, glass fiber as the separator, and a 1 *M* $NaClO_4$ solution in EC/EDC (1:1 v/v) with 5% fluoroethylene carbonate (FEC) as the electrolyte. The cathode was prepared by mixing 70% active material, 20% Super P carbon, and 10% PVDF binder in NMP, casting onto Al foil, and drying at 80°C overnight. Electrochemical testing was conducted using a Neware battery tester (MIHW-200-160CH, Shenzhen, China) over the voltage range of 2.0−4.0 V vs Na^+/Na at 1 C (120 mA g^{-1}). For high voltage stability, tests were also conducted at 2.0−4.3 V and 2.0-4.5 V (1 C = 160 mA g^{-1}). Additionally, electrochemical performance was evaluated at 55 ^oC in the voltage range of 2.0−4.0 V and 2.0−4.3 V. Galvanostatic intermittent titration (GITT) was performed with a 30-minute charge at 0.1 C followed by 10 hours of open-circuit relaxation. Cyclic voltammetry (CV) was measured using a Princeton instrument system. In the full cell system, the anode consisted of hard carbon (80%), Super P (10%), and PVDF (10%) without pre-sodiation. Galvanostatic charge/discharge tests were carried out at current densities based on the positive electrode's mass in the voltage windows of 1.9–3.9 V and 1.9–4.2 V.

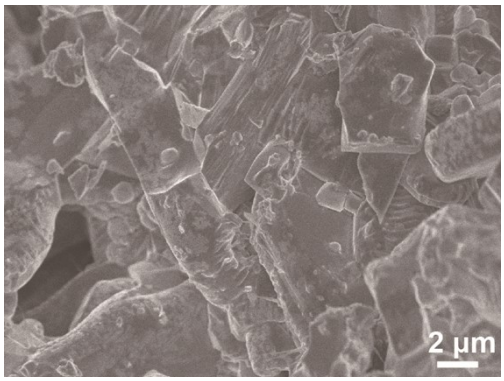

Figure S1. SEM image of NaNCMMT cathode material.

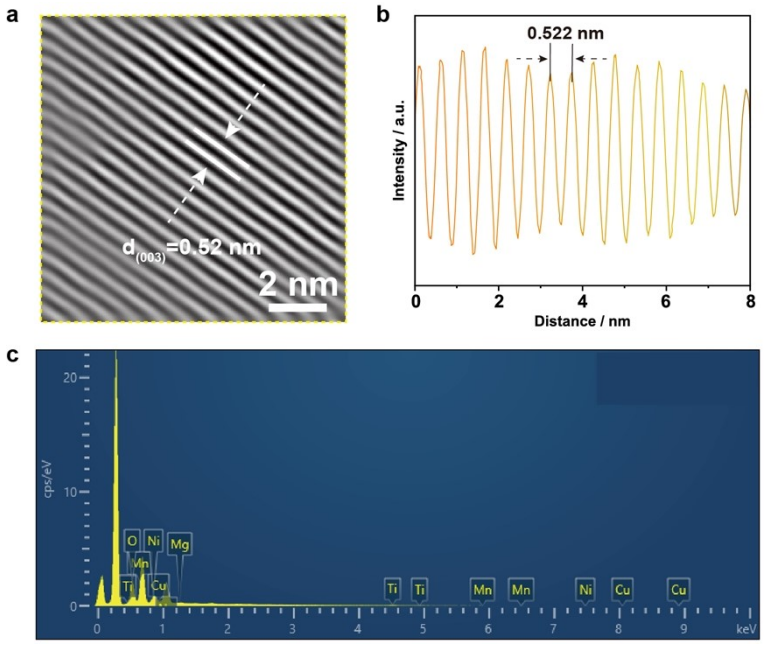

Figure S2. (a) Magnification of HR-TEM image. (b, c) Line profile of the HR-TEM image and EDS spectrum for NaNCMMT cathode material.

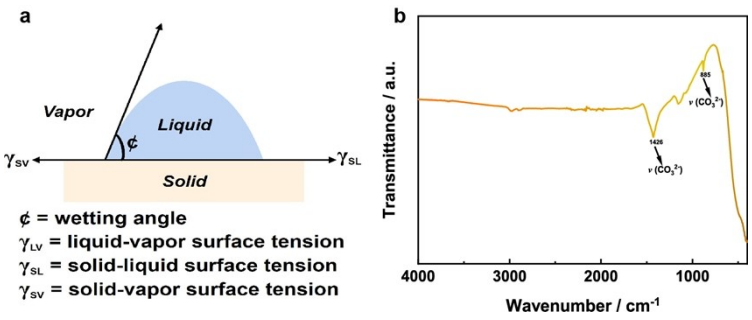

Figure S3. (a) Schematic representation of the wetting of a solid by a liquid phase. (b) IR spectra of NaNCMMT cathode material after soaking.

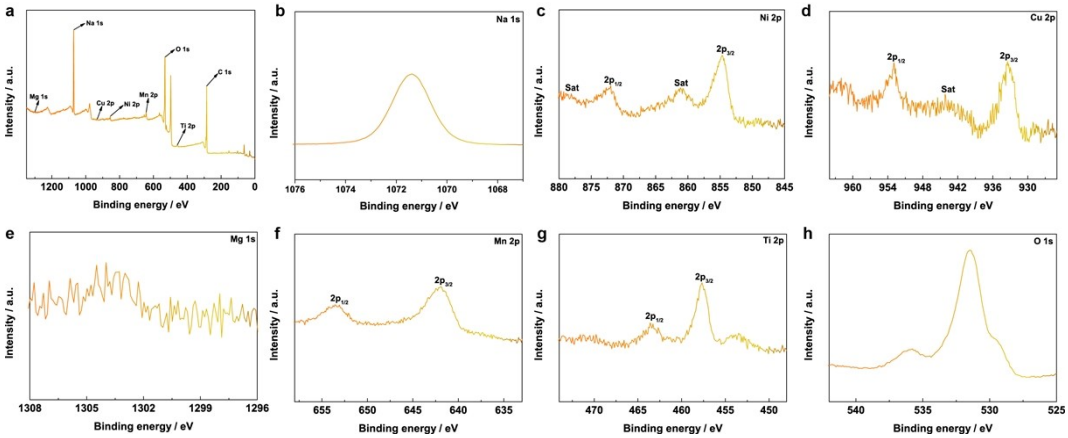

Figure S4. XPS spectra of NaNCMMT cathode material: (a) survey spectrum, (b) Na1s, (c) Ni 2p, (d) Cu 2p, (e) Mg1s, (f) Mn 2p, (g) Ti 2p, (h) O1s.

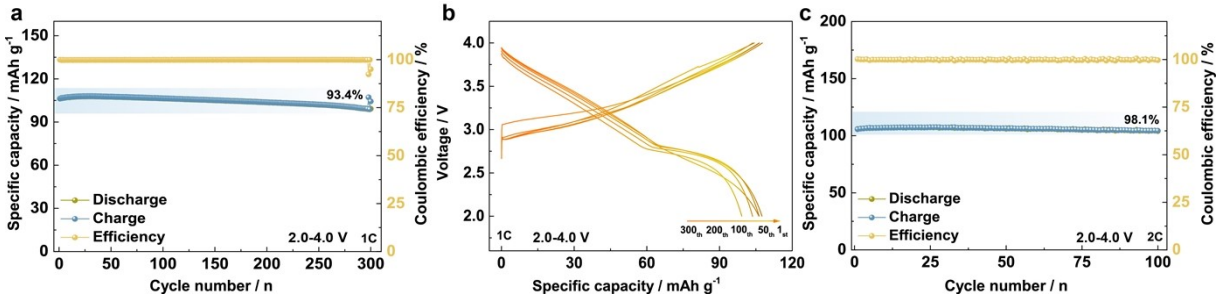

Figure S5. (a, b) Cycle performance of NaNCMMT electrode during 300 cycles and the corresponding galvanostatic charge/ discharge curves at 1 C in 2.0-4.0 V. (c) Cycle performance of NaNCMMT electrode during 100 cycles at 2 C in 2.0-4.0 V.

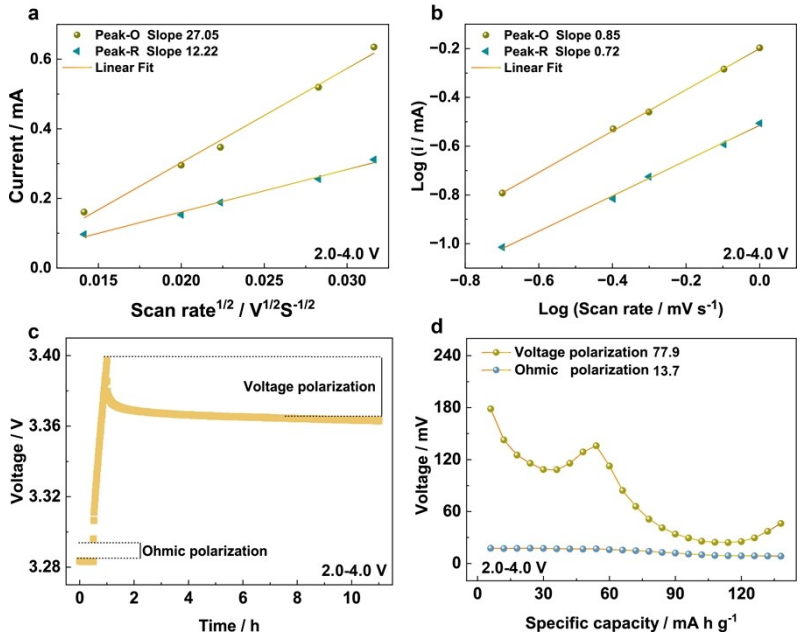

Figure S6. (a) Linear fitting of peak current versus square root of the scan rate of NaNCMMT electrode in 2.0-4.0 V. (b) Linear fitting of the log (*i*) versus log (*v*) plots of NaNCMMT electrode in 2.0-4.0 V. (c) A single step of voltage polarization with ohmic polarization of NaNCMMT electrode in 2.0-4.0 V. (d) Voltage Polarization and Ohmic Polarization of NaNCMMT electrode in 2.0-4.0 V.

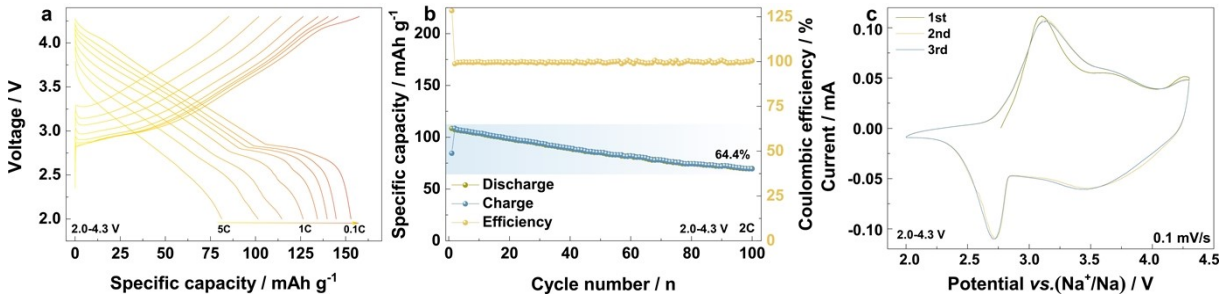

Figure S7. (a) Charge/discharge curves of NaNCMMT electrode at various rates in 2.0-4.3 V. (b) Cycle performance of NaNCMMT electrode during 300 cycles at 2 C in 2.0-4.3 V. (c) CV curves at 0.1 mV s^{-1} in 2.0-4.3 V.

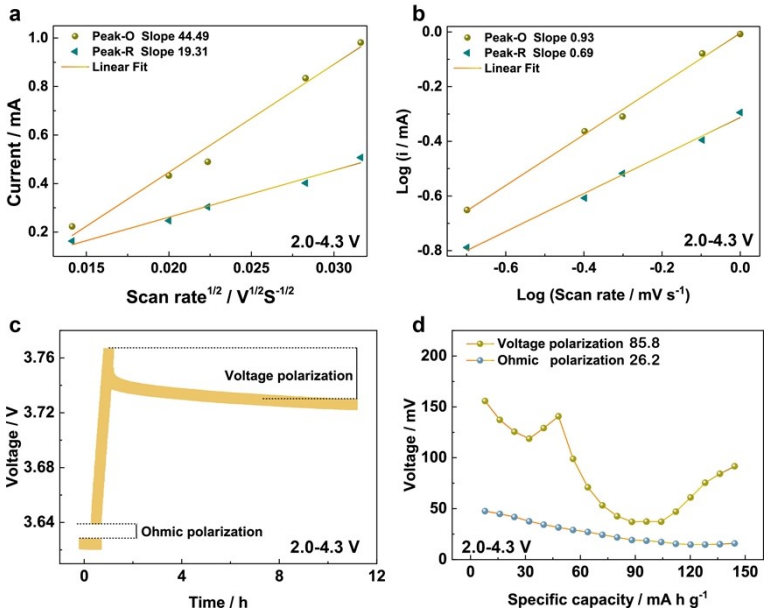

Figure S8. (a) Linear fitting of peak current versus square root of the scan rate of NaNCMMT electrode in 2.0-4.3 V. (b) Linear fitting of the log (*i*) versus log (*v*) plots of NaNCMMT electrode in 2.0-4.3 V. (c) A single step of voltage polarization with ohmic polarization of NaNCMMT electrode in 2.0-4.3 V (d) Voltage Polarization and Ohmic Polarization of NaNCMMT electrode in 2.0-4.3 V.

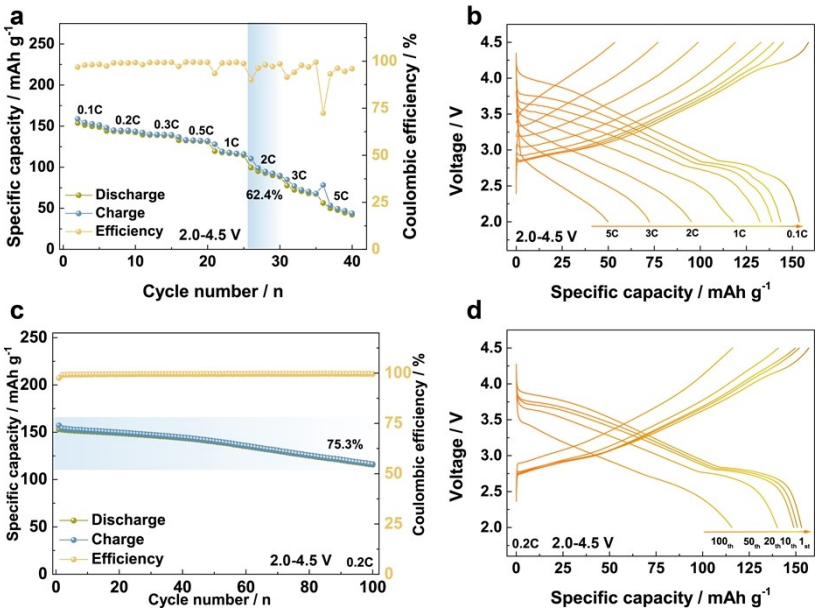

Figure S9. (a, b) Rate performance of NaNCMMT electrode at various rates and the corresponding galvanostatic charge/discharge curves in 2.0-4.5 V. (c, d) Cycle performance of NaNCMMT electrode during 100 cycles and the corresponding galvanostatic charge/discharge curves at 0.2 C in 2.0-4.5 V.

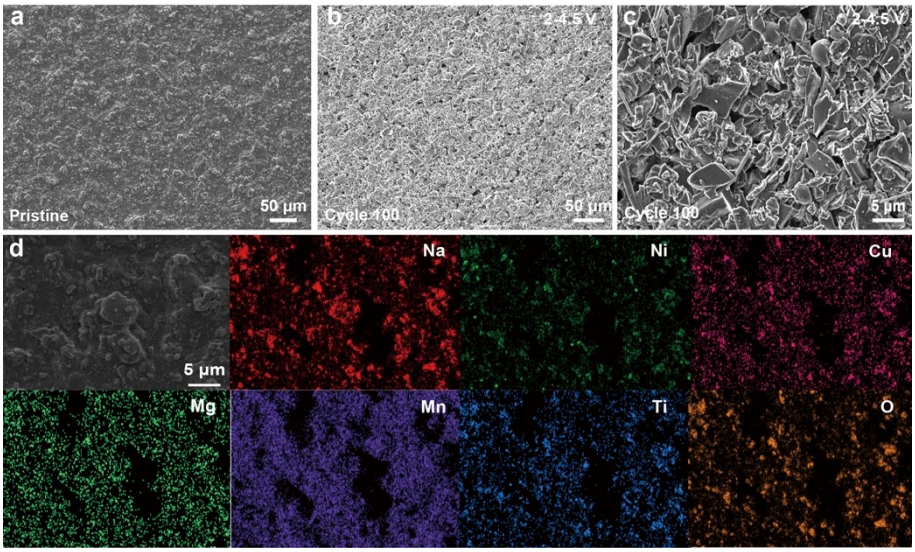

Figure S10. (a) SEM image of the pristine NaNCMMT electrode. (b, c) SEM images at different magnifications of the NaNCMMT electrode during 100 cycles charged to 4.5 V. (d) EDS mapping of Na, Ni, Cu, Mg, Mn, Ti, O elements.

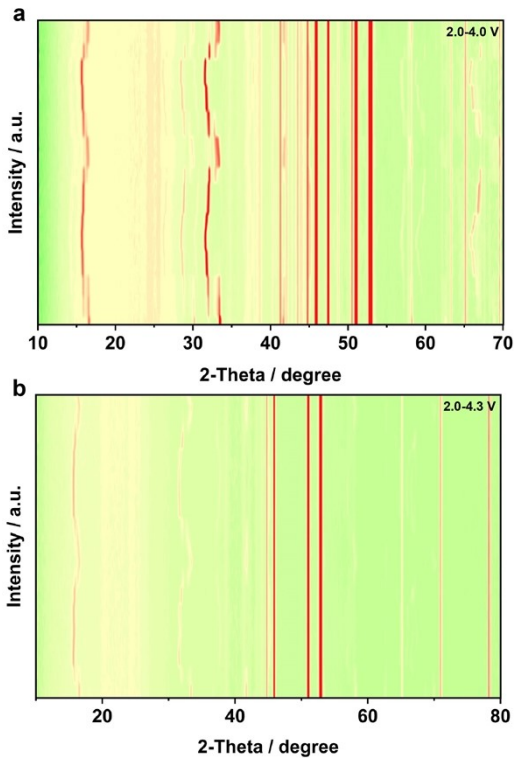

Figure S11. Intensity contour maps (bird's-eye view) of the NaNCMMT electrode during the first two charge/discharge cycles at 0.1C in the voltage ranges of 2.0–4.0 V and 2.0–4.3 V, respectively.

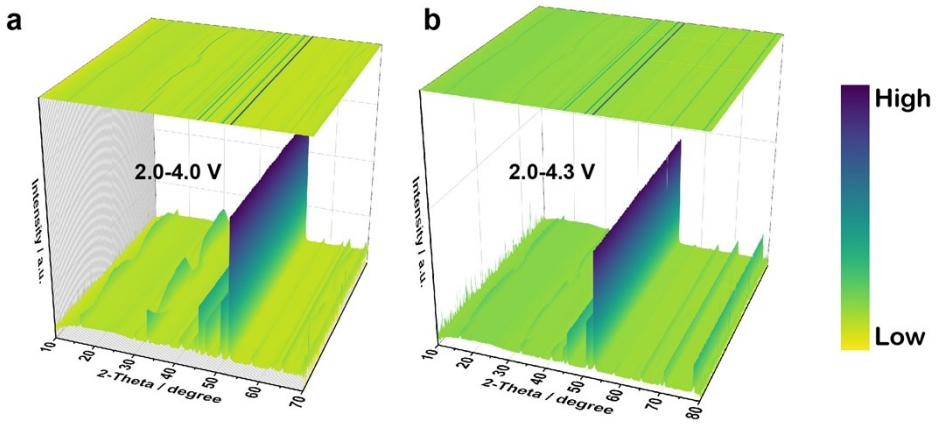

Figure S12. (a, b) The 3D counter graphs of the NaNCMMT electrode during the first two charge/discharge cycles at 0.1C in the voltage ranges of 2.0–4.0 V and 2.0–4.3 V, respectively.

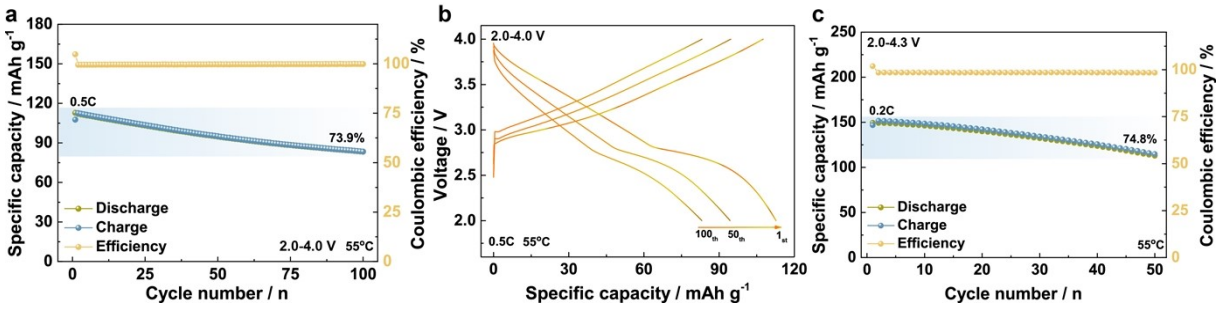

Figure S13. High temperature (55 °C) electrochemical performance of the NaNCMMT electrode. (a) Cycle performance during 100 cycles at 0.5 C in 2.0-4.0 V. (b) The corresponding galvanostatic charge/discharge curves at 0.5 C in 2.0-4.0 V. (c) Cycle performance during 50 cycles at 0.2 C in 2.0-4.3 V.

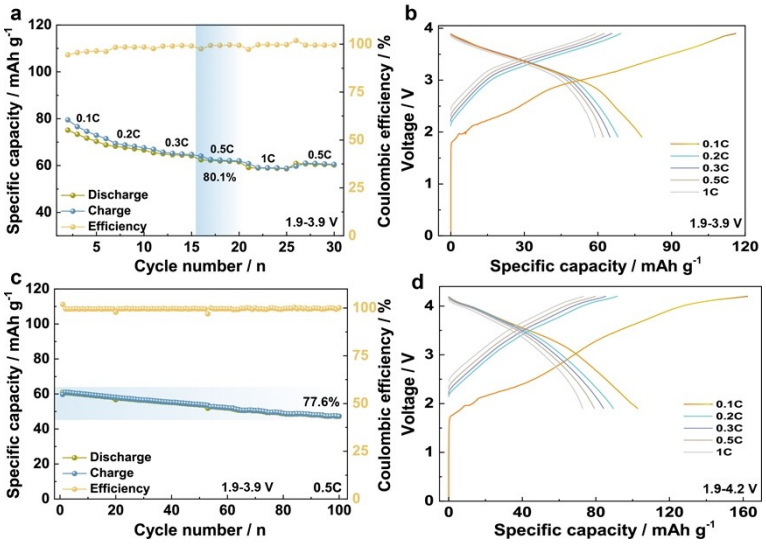

Figure S14. Electrochemical properties of a full battery system (NaNCMMT as cathode and hard carbon as anode). (a, b) Rate performance at various rates and the corresponding galvanostatic charge/discharge curves in 1.9-3.9 V. (c) Cycle performance during 100 cycles at 0.5 C in 1.9-3.9 V. (d) The corresponding galvanostatic charge/ discharge curves at various rates in 1.9-4.2 V.

Figure S15. The production process of industrial grade NaNCMMT cathode materials.

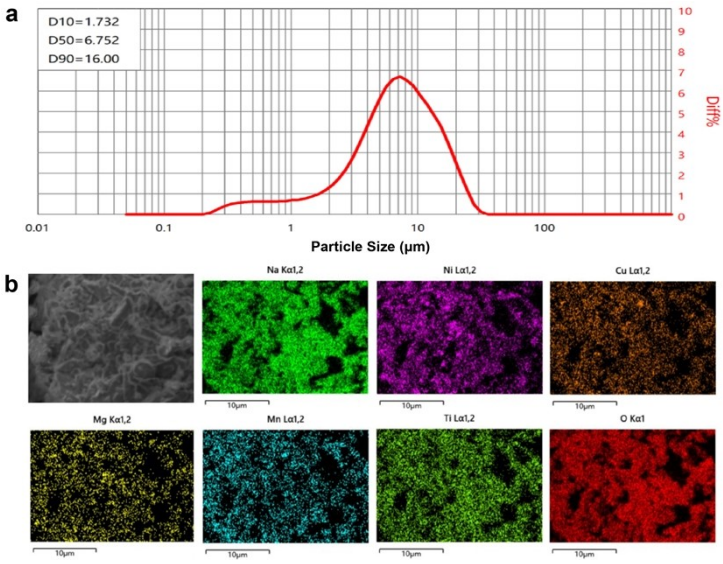

Figure S16. (a) Particle size distribution of industrial-grade NaNCMMT cathode materials. (b) EDS mapping of Na, Ni, Cu, Mg, Mn, Ti, O elements.

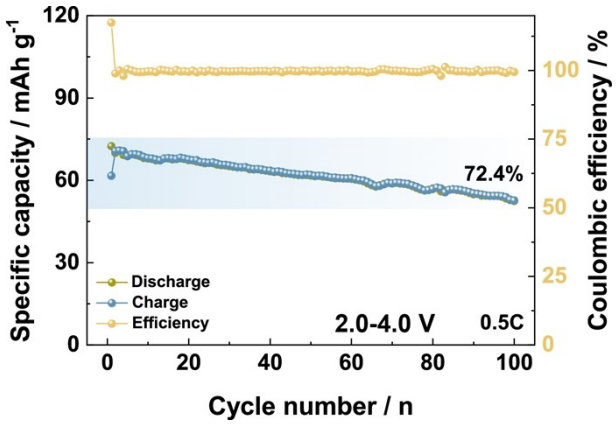

Figure S17. Cycle performance of industrial-grade NaNCMMT cathode materials during 100 cycles at 0.5 C in 2.0–4.0 V.

Table S1. The ICP-MS result of NaNCMMT cathode material.

Theoretical chemical formula	Measured atomic ratio					
	Na	**Ni**	**Cu**	**Mg**	**Mn**	**Ti**
$NaNi_{0.4}Cu_{0.05}Mg_{0.05}Mn_{0.3}Ti_{0.2}O_2$	0.992	0.406	0.051	0.048	0.302	0.196

Table S2. Contact angle result of the NaNM cathode material.

Time (s)	Left angle (°)	Right angle (°)	Average angle (°)
0	68.4	67.26	67.83
0.73	68.59	67.96	68.28
1.47	68.75	67.77	68.26
2.21	68.51	67.92	68.22
2.94	68.36	67.21	67.79

Table S3. Contact angle result of the NaNCMMT cathode material.

Time (s)	Left angle (°)	Right angle (°)	Average angle (°)
0	96.5	94.64	95.57
0.73	95.34	96.35	95.85
1.47	96.43	97.27	96.85
2.2	97.33	96.26	96.8
2.93	92.92	95.62	94.27